In-Pile Irradiation Induced Defects and the Effect on Thermal Diffusivity of MgO

Donald T. Moore[a], Cynthia A. Papesch[b], Brandon D. Miller[b], Pavel G. Medvedev[b], and Juan C. Nino[a,*]

[a]Department of Materials Science and Engineering, University of Florida, Gainesville, FL 32611, United States

[b]Idaho National Laboratory, Idaho Falls, ID 83415, United States

* Corresponding author. Tel.: +1 352 846 3787; fax: +1 352 846 3355.

E-mail address: jnino@mse.ufl.edu (J.C. Nino).

Abstract

The effects of neutron irradiation temperature and dose on thermal diffusivity are compared between non-irradiated and in-pile irradiated MgO samples. MgO pellets were irradiated in-pile of the Advanced Test Reactor at Idaho National Laboratory. Samples were irradiated at 623 and 973 K to fast neutron fluences of 1 x 10^{25} (1.5 dpa) and 2 x 10^{25} n/m^2 (3 dpa). Post irradiation examination included X-ray diffraction, scanning electron microscopy, laser flash thermal diffusivity, and transmission electron microscopy. The radiation induced thermophysical and structural evolution of MgO is reported.

1. Introduction

There is an increasing radiotoxic inventory of nuclear waste including plutonium from both spent nuclear fuels and dismantled nuclear weapons and minor actinides

such as neptunium, americium, and curium from spent nuclear fuel [1]. Geological disposal requires storage for thousands of years due to long half-life's of Pu and minor actinides [2]. An approach for reducing nuclear waste while utilizing their energetic value is by using a mixed oxide fuel (MOX) or an inert matrix fuel (IMF) for the transmutation of waste in light water reactors (LWRs) or fast reactors [3]. Mixed oxide fuels contain uranium and plutonium or other actinides, but these fertile matrices results in neutron capture generating additional plutonium and actinides [4]. An inert matrix fuel consists of a non-fertile inert matrix (IM) that supports a fissile phase (Pu or minor actinides) for efficient transmutation. The IM can be metal or ceramic and can be a single phase or multiphase material [5].

Magnesium oxide (MgO) has many of the properties desired for IMF such as high thermal conductivity (30 W/mK at 773 K [6]), high melting point (3073 K [7]), low neutron absorption cross section, and good radiation tolerance. Magnesium oxide, also known as magnesia or periclase, has a rocksalt crystal structure represented by interpenetrating fcc lattices and has a space group of $Fm\bar{3}m$ (No. 225). Light anions and cations of similar atomic weight with a simple crystal structure typically lead to a high thermal conductivity as in MgO. More now than ever, a critical requirement in the search of new materials is that of accident-tolerant fuels for LWRs [8]. For example, in the event of a fuel pin failure, the IM needs to be compatible with the reactor coolant. Unfortunately, MgO is soluble in hot water, thus limiting its use as a single-phase inert matrix material due to its poor hydration resistance for use in LWRs. However, it has been demonstrated that a multiphase composite approach could yield sufficient hydration resistance for use of MgO in LWRs; e.g. MgO-ZrO_2 [9] and MgO-$Nd_2Zr_2O_7$

[10]. MgO is also being studied as a promising matrix for burning PuO_2 and actinides such as AmO_{2-x} in fast reactors [11], that do not use water as the primary coolant.

Since MgO can be used as a composite in IMFs for LWRs or as the inert matrix in IMFs for fast reactors, it is important to understand the effects of irradiation damage on the thermophysical properties under different irradiation conditions. There are several studies on the low temperature thermal conductivity of neutron irradiated MgO [12-14], but there is limited information on the effect of in-pile irradiation damage on the thermal diffusivity or conductivity at high temperatures of MgO. Therefore, additional research is needed to understand how irradiation damage affects the thermophysical properties of MgO. This experiment provides a constant comparison of MgO before and after in-pile irradiation at 623 and 973 K. This paper will discuss the effects of irradiation damage on the thermal diffusivity of MgO.

2. Experimental procedure

2.1. Pellet fabrication

Commercial MgO (Cerac 99.9%) was ball milled with 70 ml of anhydrous ethanol (Fisher A405). The slurry was milled for 24 h then dried in a fume hood at ambient conditions overnight. In a porcelain mortar and pestle, 2 wt% of binder (Celvol 103 Polyvinyl Alcohol, PVA) was added to the MgO powder and ground to combine thoroughly then sieved through a 212 μm mesh. The sieved powder was then dried at 393 K for 5 min to remove moisture. The powder was uniaxially pressed at 180 MPa then sintered in air at 1923 K for 12 h.

For thermal diffusivity samples, pellets were sintered into 6 mm diameter pellets ~1.8 mm thick. For transmission electron microscopy (TEM) samples, pellets 3 mm in diameter were cut using an ultrasonic drill from an 11 mm diameter and ~1.0 mm thick sintered pellet. The weight and dimensions of the pellets were measured using a balance, caliper, and micrometer then the geometric density was calculated.

2.2. Irradiation conditions

To control the temperature at which the samples were irradiated, the capsules were back filled with either 100% helium for the low temperature (~623 K) or 15% helium and 85% argon for the high temperature (~973 K). The irradiation temperature was calculated using ABAQUS 6.7-3 [15]. The samples were then irradiated in position B-1 of the Advanced Test Reactor at Idaho National Laboratory to fast neutron fluencies of ~1 x 10^{25} (150 effective full power days) and ~2 x 10^{25} n/m^2 (297 days) [16, 17]. The displacements per atom were calculated using MCNP and determined to be approximately 1.5 and 3 dpa for a displacement energy of 55 eV [18] used for MgO. Table 1 has the sample identifications for the different irradiation conditions (I1-3) and non-irradiated (N) used throughout the paper and Figure 1 has the results from the minimum irradiation temperature and displacement calculations. The slight differences in temperature (±50 K) and displacements per atom (±0.1 dpa) between the TEM and diffusivity samples are due to the different sample holders and height within the reactor core. For the purposes of the analysis, it was assumed that irradiation conditions of the TEM and diffusivity samples were equivalent.

Table 1. MgO Irradiation conditions and identification.

Label	Sample	$T_{irr,min}$ (K)	Displacements (dpa)
N	-	-	-
I1	TEM	641	1.56
	Disk	580	1.54
I2	TEM	626	2.99
	Disk	582	3.07
I3	TEM	972	3.17
	Disk	932	3.16

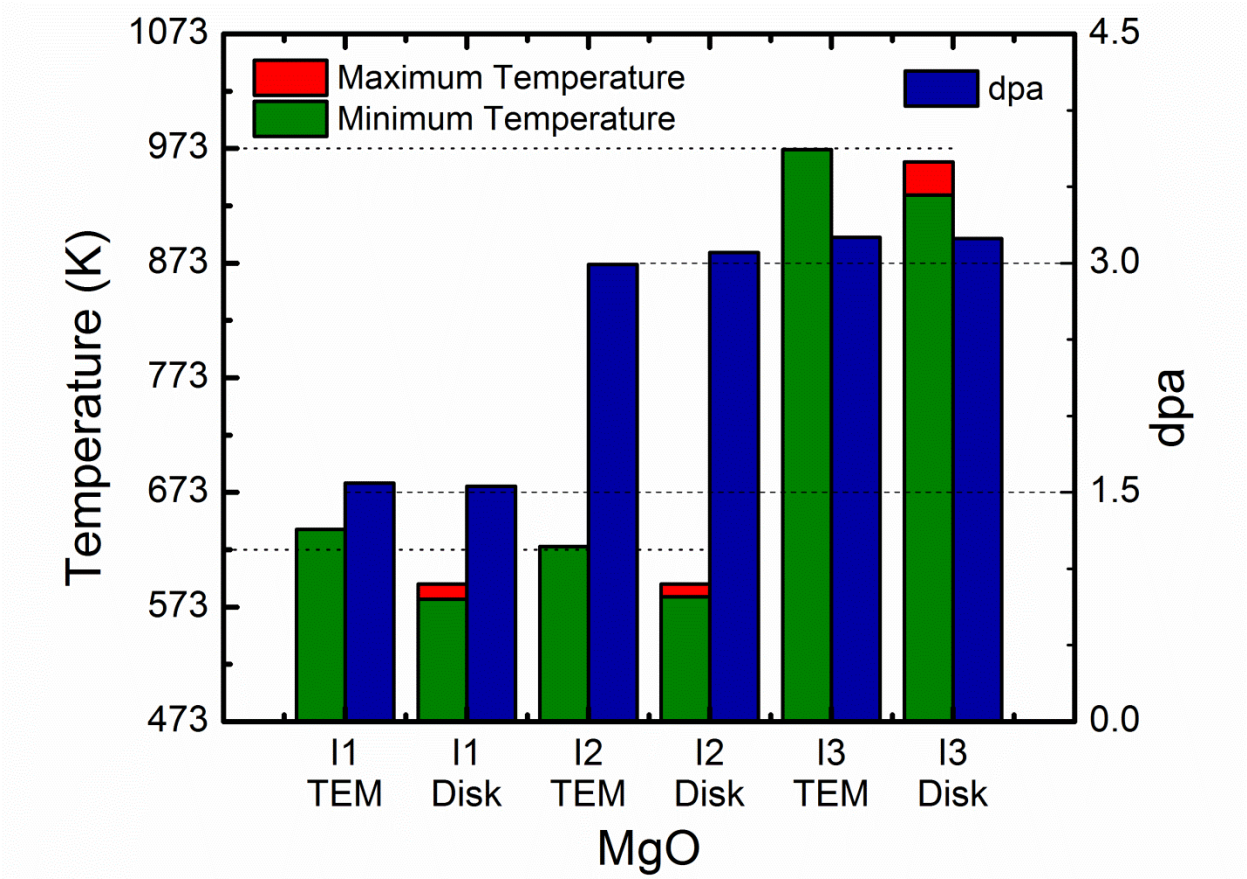

Figure 1. Irradiation temperatures (green and red) and dpa (blue) calculations for MgO in capsules I1, I2, and I3.

2.3. Post-irradiation examination

2.3.1. X-ray diffraction and scanning electron microscopy

Capsules were disassembled and categorized in the Hot Fuel Examination Facility at Idaho National Laboratory. Samples were decontaminated in a fume hood by grinding with 400 grit SiC paper and cleaning with acetone. The crystal structure of as-sintered and out-of-pile pellets was characterized by benchtop powder X-ray diffraction (XRD, Inel Equinox 1000, Artenay, France). The XRD was conducted using CuKα radiation and the operation power for the generator was set to 40 kV and 30 mA.

Polished and thermal etched N-MgO and fractured cross sections of N and I1 pellets were examined using scanning electron microscope (SEM) at 15 kV (JEOL JCM-5000, Tokyo, Japan; Zeiss 1455 VP Maple Grove, MN).

2.3.2. Focused ion beam and transmission electron microscopy

The TEM specimens were prepared by dual-beam focused ion beam (FIB, FEI Quanta 3D FEG FIB/SEM, Hillsboro, OR) to final lamella dimensions of 10 x 8 μm by ~100 nm thickness. A 2 μm thick platinum layer was deposited and trenches were then milled. The specimen was coarse milled at an accelerating voltage of 30 kV and a beam current of 7 nA to a thickness of 2 μm then at 3 nA to an 1 μm thickness. The specimen was cut and lifted out using an omniprobe then fixed to a TEM grid using Pt deposition. Care was taken not to damage the sample with the ion beam and to use a low energy cleaning to minimize ion damage. The sample was thinned with 30kV and 300 pA to 120 nm. The sample was then cleaned using 5 kV and 150 pA, 5 kV and 77 pA, and a final cleaning using 2 kV and 86 pA to the final thickness.

Bright field (BF) images, two-beam images, and selected-area electron diffraction (SAED) patterns were recorded using TEM at room temperature (JEOL 2010F, Tokyo, Japan) operated at 300 kV.

Pellets from I2 and I3 were annealed in a graphite furnace (RDWEBB RD-G, Natick, MA) at 1673 K in a flowing argon atmosphere for 1 h, and were then milled using the FIB to prepare a TEM lamella.

2.3.3. Laser flash thermal diffusivity

The thermal diffusivity of the samples was measured according to ASTM standard E1461-07 using the laser flash technique (Anter Flashline 5000 installed in a glove box, Pittsburgh, PA). All samples were mechanically thinned with 320 grit SiC paper to 1 mm. Since MgO is translucent, the surfaces were sputter coated with gold and then sprayed with a thin coat of graphite. One sample of each irradiation condition was measured under flowing argon during the same experiment with a multiple sample carousel. Three measurements of each sample were taken at 297 K and from 373 K to 873 K at 100 K intervals. The diffusivity was calculated following the Clark and Taylor correction for all samples [19].

3. Results and discussion

3.1.1. Color centers, crystal structure, and microstructure

Upon visual inspection, it was clear that none of the twelve 6 mm and eight 3mm diameter MgO pellets cracked after irradiation. However, the pellets changed color from white to black as shown in Figure 2. Samples were fractured and the color change was uniform throughout the thickness of the sample as expected. The observed color change is consistent with the occurrence of F+ centers in MgO, whose concentration increases with increasing neutron fluence until a saturation level of 1.3×10^{23} m^2 [20]. After annealing in flowing argon at 1673 K for 1 h (same atmosphere as thermal

diffusivity measurements and similar to the 85%Ar/15%He I3 backfill gas), the I2 and I3 sample color changed to a grey color indicating the slight reduction in the concentration of F+ centers. The thermal anneal was under argon and therefore reoxidation is not expected, as evidenced by the remaining grey color. As will be shown later in this article, TEM analysis indicated that the recovery was due vacancy-interstitial recombination, interstitial dislocation growth, and coalescence of vacancies into voids.

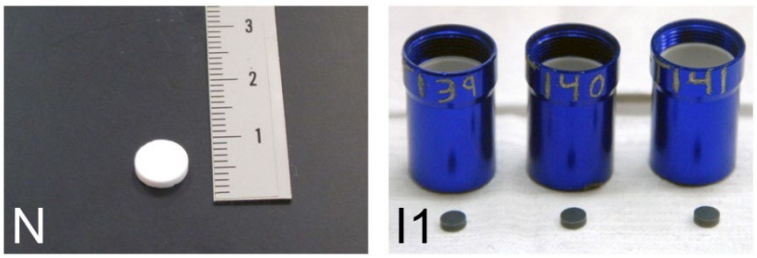

Figure 2. Optical images of non-irradiated (white) and irradiated (black) MgO pellets.

X-ray diffraction normally allows for calculating dislocation density from strain-induced peak broadening [21]. However, at low doses in MgO, damage is expected to be mainly comprised of Frenkel defects, while at higher doses or upon annealing, interstitial defects coalesce into dislocation loops. It has been shown that large size or high number of interstitial loops causes the Bragg peak to disappear at 2 x 10^{24} n/m^2 for MgO and a rather sharp peak forms due to diffuse scattering near the location of the Bragg peak [22]. Since, as it will be discussed later, TEM shows that there are large dislocation loops and thus as previously described, it can be concluded that the peaks are due to diffuse scattering and not Bragg scattering. Consequently, the peak broadening and shift towards smaller 2θ observed in the Figure 1 inset is due to diffuse scattering, and therefore, conventional strain, lattice parameter change, or swelling

calculations from XRD profiles were not performed. Nonetheless, as a first approximation, the XRD patterns in Figure 3 indicate that there was no phase change or extensive amorphization due to irradiation. This is corroborated by the slope of the inverse thermal diffusivity shown later, which remained unchanged with irradiation meaning there was no change in the intrinsic thermal diffusivity.

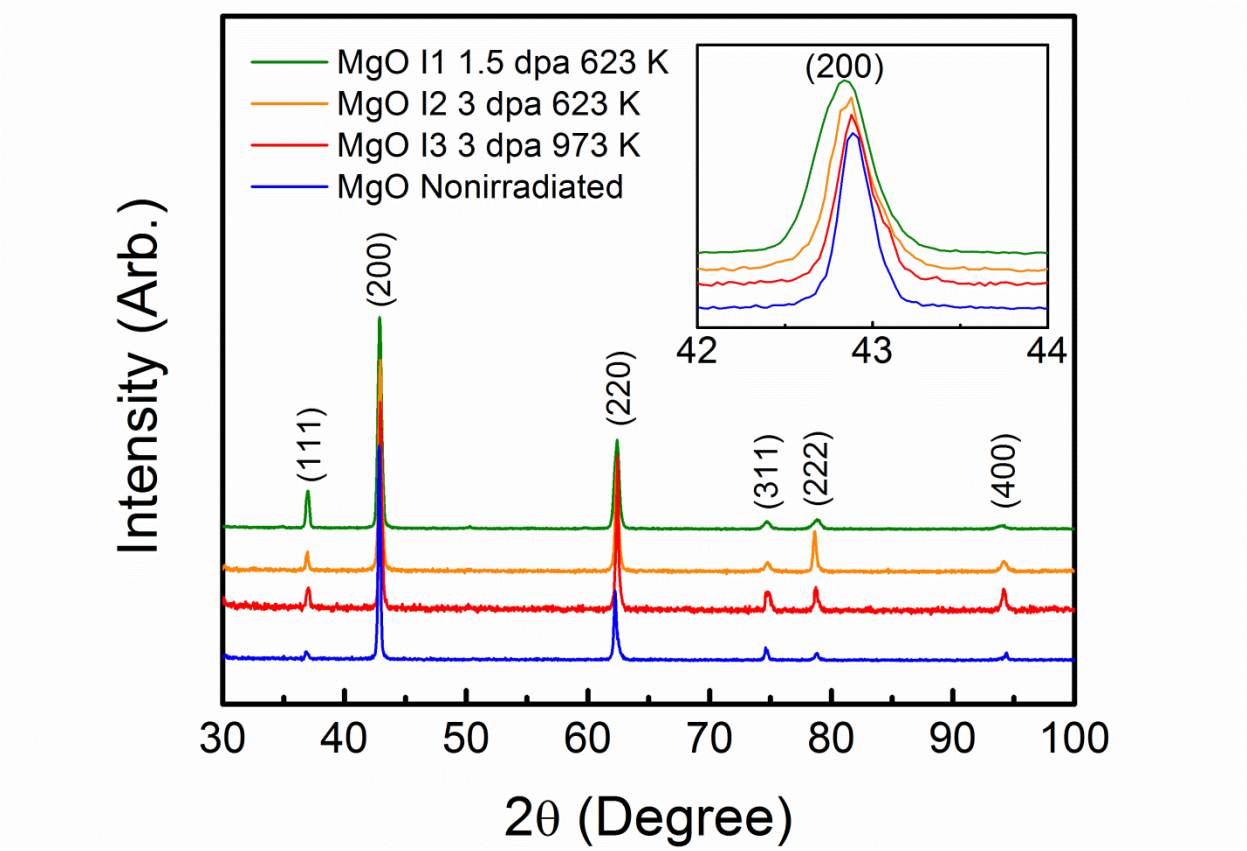

Figure 3. XRD patterns of MgO showing that the material did not amorphize or change phase during irradiation. The inset shows peak broadening and shift due to diffuse scattering caused by irradiation damage.

The average grain diameter for the samples before irradiation using the ASTM E112-10 intercept procedure was determined to be 11(±1) μm from Figure 4 (top N). There are some large grains due to irregular grain growth. Grain growth was not

observed in the irradiated samples. In-pile neutron irradiated MgO exhibits transgranular fracture suggesting a decrease in fracture toughness [23]. The non-irradiated MgO exhibited intergranular fracture through pores on the grain boundaries. The irradiated I1 MgO sample exhibited transgranular fracture and the change can be attributed to the grains becoming more brittle than the grain boundary due to the high density of dislocations caused by irradiation.

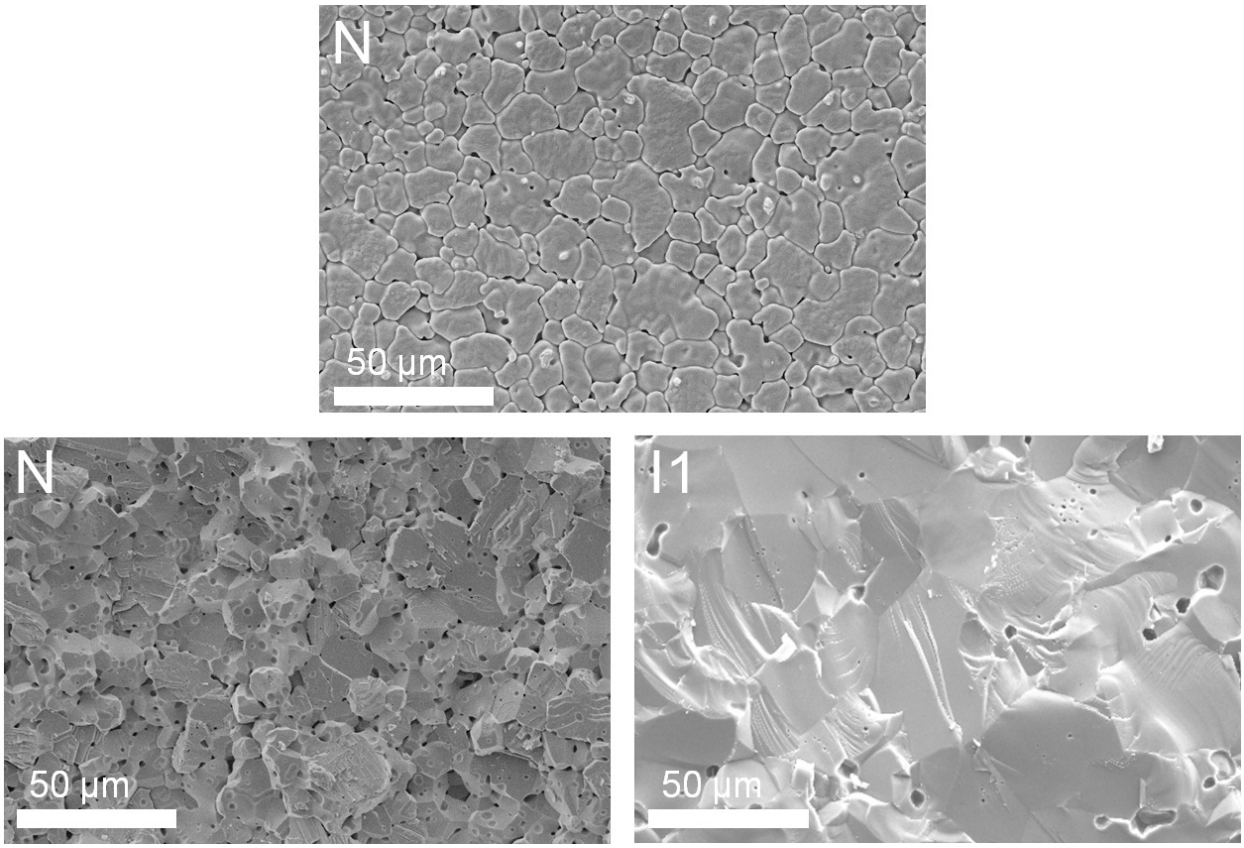

Figure 4. SEM (top) of thermally etched, non-irradiated MgO microstructure. The SEM (left) of non-irradiated MgO shows intergranular fracture and the SEM (right) of I1 MgO shows transgranular fracture.

A neutron irradiation study of MgO reported swelling of 2.6-3 vol% for 30 dpa at 430 K due to voids [24], which is an order of magnitude greater dpa than in this study.

Sample dimensions were measured geometrically for the thermal diffusivity measurements. All of the samples had an average density of 98% before irradiation and after irradiation. Geometric densities were not accurate enough to determine swelling since the error in geometric densities was calculated to be 2% for the 6 mm samples. Small voids were seen in TEM along grain boundaries in I3 and not in I2 indicating that swelling is greater at the higher irradiation temperature.

3.1.2. Thermal diffusivity

The thermal conductivity (κ) of a material and the lattice thermal conductivity (κ_L) can be calculated by the following equations:

$$\kappa = \alpha C_p \rho \tag{1}$$

$$\kappa_L = \frac{1}{3} C_v v l_{tot} \rho \tag{2}$$

where α is the thermal diffusivity, $C_{p,v}$ is the specific heat at constant pressure or volume, and ρ is the density. Setting the above two equations equal, the thermal diffusivity can be expressed as:

$$\alpha = \frac{1}{3} v_s l_{tot} \tag{3}$$

where v is the average phonon velocity, which is approximately constant with temperature and l_{tot} is the total mean free path of the phonons, which can be described by the following equation for irradiated materials:

$$\frac{1}{l_{tot}} = \frac{1}{l_{pp}} + \frac{1}{l_n} + \frac{1}{l_i} \tag{4}$$

where l_{pp} is the mean free path due to phonon-phonon scattering (intrinsic lattice diffusivity), l_n is mean free path due to defects present before irradiation, l_i is the mean

free path due to irradiation-induced defects [25]. The inverse diffusivity can thus be modeled by a linear relationship with temperature:

$$\frac{1}{\alpha} = AT + B \tag{5}$$

where *A* is related to temperature dependent phonon-phonon scattering and *B* is related to the temperature independent phonon scattering by defects such as grain boundaries, impurities, dislocations, etc [26].

Thermal diffusivity of neutron-irradiated ceramics depends on the measured T (K) by the following empirical fit:

$$\alpha = k / T^n \tag{6}$$

where k is a constant related the absolute value, and n is a constant that represents the state of the induced defects [27]. Neutron irradiation produces large defects, which can be seen with the electron microscope, and point defects, which account for large changes in thermal conductivity [28]. In Figure 6, the thermal diffusivity of non-irradiated MgO and irradiated MgO was fitted to equation 6. Both MgO I1 and I2 have the most significant reduction in thermal diffusivity due to the high density of small dislocations. Nonetheless, there is little change with the increased irradiation dose. The saturation dose for thermal diffusivity or conductivity is not known for MgO. The saturation dose is important since the diffusivity will not decrease further with increasing dose. Since there is a small reduction in thermal diffusivity between I1 and I2, the saturation dose has not been reached for MgO in this study and thus can be taken as higher than 3.07 dpa at 580 K. MgO I3 irradiated at high temperature has an intermediate decrease in thermal diffusivity compared to N and I1 because of a lower

density and larger size of dislocations. The distance between defect clusters increases with increasing irradiation temperature due to recombination [29]. At higher temperatures, the difference in thermal diffusivity between irradiation conditions decreases. The MgO samples were measured on heating and upon reaching higher temperatures, the I1 and I2 began to anneal and recover towards the thermal diffusivity of the I3 MgO.

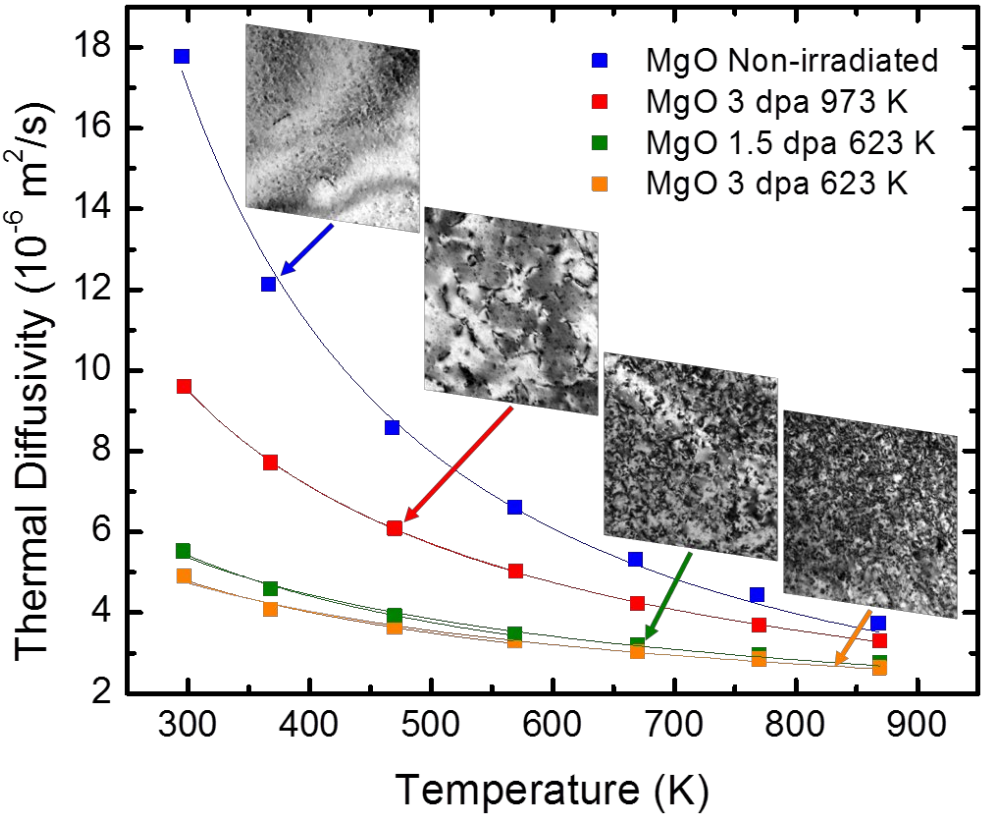

Figure 5. Thermal diffusivity of non-irradiated MgO (blue) compared to MgO at different irradiation conditions. Both MgO I1 (green) and I2 (orange) have the most significant reduction in thermal diffusivity due to the high density of small dislocations. I3 (red) irradiated at high temperature has an intermediate decrease in thermal diffusivity because of the lower density and larger size of the dislocations.

The thermal diffusivity of the measured samples was fitted to equation 6 and the fitting parameters are listed in Table 2. The fit was performed twice to compare fitting the measurements from room temperature up to 573 K (bellow the irradiation temperature of 623 K) and up to 873 K (above the irradiation temperature of 623 K) for I1 and I2 samples. The annealing during the measurement had a slight decrease in n for the I1 and I2 samples, which incorrectly overestimated the induced defects caused by irradiation. Therefore, to calculate the diffusivity at the irradiation temperature, α_{irr}, the n_{873} was used for the I3 and n_{573} was used for I1 and I2, such that the fit was to measured values below the irradiation temperatures. Therefore, to more accurately and (thus safely) predict the thermal diffusivity at operating conditions, it is clear that the thermal diffusivity should be measured up to the irradiation temperature, and not above. This would incorrectly increase the calculated thermal diffusivity due to defect annealing (recovery) during the measurement. The samples should also be irradiated as close to the operating conditions to determine correctly the thermal diffusivity because defects vary greatly with irradiation temperature and dose. Since the thermal diffusivity is measured out-of-pile, it is assumed that the post irradiated samples have the same amount of defects during irradiation, that additional defects were not introduced at lower temperature while cooling down the reactor, and that defects remain stable during the measurements up to the irradiation temperature. The thermal diffusivity at the irradiation temperature was calculated by the following equation and values are listed in Table 2:

$$\alpha_{irr} = \alpha_{297}\left(297 / T_{irr}\right)^{n} \tag{7}$$

Table 2. Thermal diffusivity fitting parameters and diffusivity at irradiation temperature.

Sample	Dose (10^{25} n/m^2)	T_{irr}	n_{573}	n_{873}	α_{297} (10^{-6} m^2/s)	α_{irr} (10^{-6} m^2/s) from n_{573}	α_{irr} (10^{-6} m^2/s) from n_{873}
Non-irradiated			-	1.48(5)	17.78	-	-
I3	2	973	0.993(7)	0.999(4)	9.60	2.95	**2.93**
I1	1	623	0.71(3)	0.65(2)	5.52	**3.26**	3.41
I2	2	623	0.61(7)	0.56(3)	4.90	**3.12**	3.24

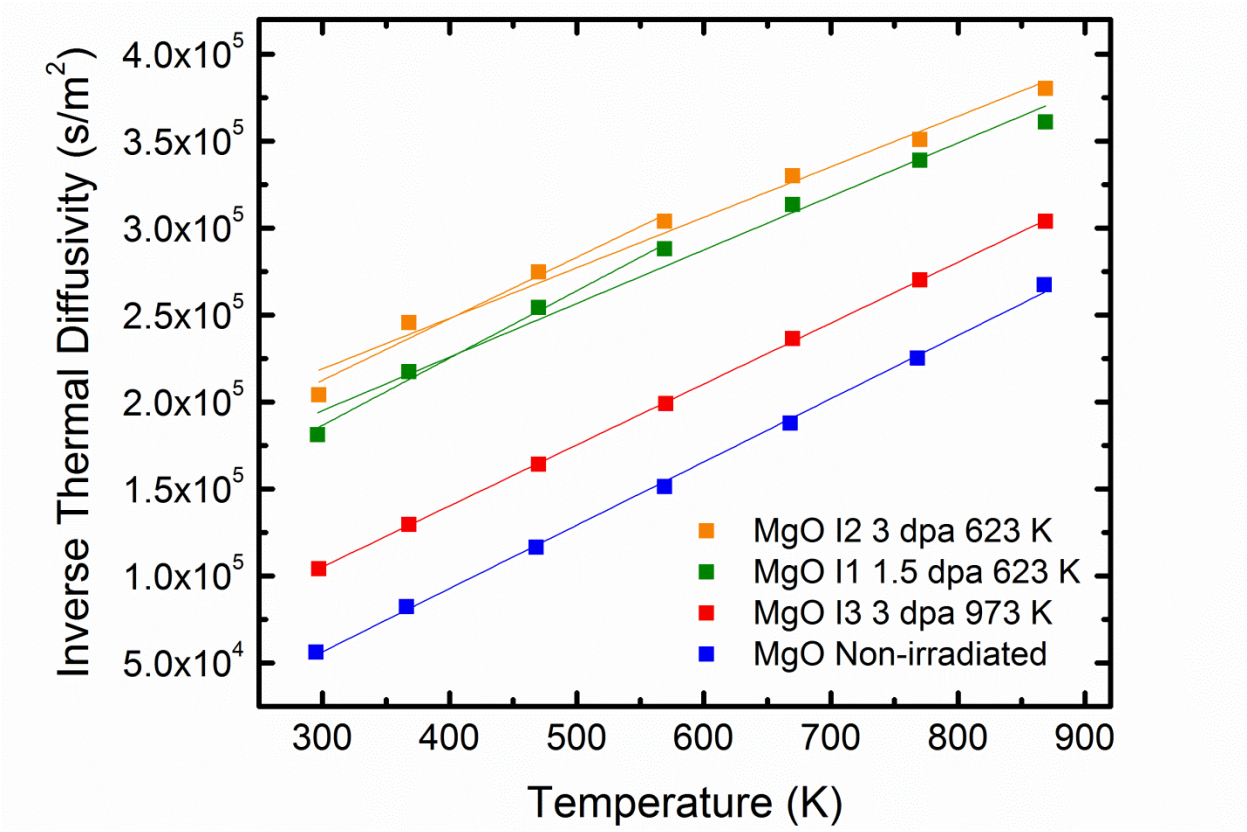

Figure 6. Inverse thermal diffusivity with linear fit from room temperature to 573 and to 873 K. Fitting measured diffusivity values above the irradiation temperature results in an apparent decrease in the intrinsic lattice diffusivity (slope).

To better understand the change in *n*, linear extrapolation of the measured inverse diffusivity versus absolute temperature gives a slope (that is determined by the lattice) and the intercept at 0 K (chiefly determined by defects) [26]. The inverse

thermal diffusivity linear fit (equation 5) was performed twice with the same temperature ranges as before. For I1 and I2 in Figure 7, when fitting using the data above the irradiation temperature, this led to an apparent decrease in the slope, which is the intrinsic lattice diffusivity, and an apparent increase in the intercept, which is due to defects. Table 3 has the results of the inverse fit up to but not above the irradiation temperature. By fitting up to the irradiation temperature, the slope (average of 363 s/m^2K) remains unchanged due to irradiation conditions, indicating no change in phonon-phonon scattering. The intercept, which indicates the number of defects, increased with irradiation dose and decreased with the higher irradiation temperature because point defects are more effective as scattering than aggregates. Higher irradiation temperatures result in greater aggregation and thus less scattering [23].

Table 3. Inverse diffusivity slope (lattice) and intercept (defects) of irradiated MgO.

Sample	Dose (10^{25} n/m^2)	T_{irr}	Slope (s/m^2K)	Intercept (s/m^2)	Adj. R-Square
Non-irradiated			363(6)	-52(3) x 10^3	0.9985
I3	2	973	350(2)	8(10) x 10^2	0.9999
I1	1	623	386(23)	70(10) x 10^3	0.9893
I2	2	623	353(42)	106(19) x 10^3	0.9571
		Mean	363		

3.1.3. Transmission electron microscopy

Dislocation formation in MgO is well studied and is characterized by dislocation loops and tangles [30]. Typically, interstitial loops that lie on the {110} planes have <110> Burgers vectors and often intersect forming dislocation tangles [30]. Low temperature irradiation of MgO normally results in unfaulted, elongated interstitial loops at higher doses [24]. Here, TEM images of MgO in Figure 5 show that at the low irradiation temperatures (I1 and I2) there is a high density of small dislocations, which increased with the higher irradiation dose. The higher irradiation temperature (I3) leads

to a lower density of larger dislocations. It is anticipated that the higher irradiation temperature increased interstitial diffusion leading to aggregation of dislocation, which can be seen by the lack of damage around dislocation structures. The higher irradiation temperature also increases recombination resulting in a lower dislocation density. It can be seen that the I3 MgO samples has tangled dislocations and a few dislocation loops. Conversely, at the low irradiation temperatures, point defects were not mobile enough to recombine or make larger defects and led to the high defect density, which caused the most significant decrease in thermal diffusivity. The density of the dislocations was calculated by the line intercept method and determined to be 1.0, 2.4, and 4.5 x 10^{14} m^{-2} for I3, I1, and I2 respectively. Although not presented here, TEM also showed the presence of ~1 nm voids at the grain boundary of I3 MgO but voids in the bulk were not resolvable. There were no resolvable voids at the grain boundaries or in the bulk of I2 MgO. Two-beam imaging was performed to attain an overall representation of the total irradiation damage.

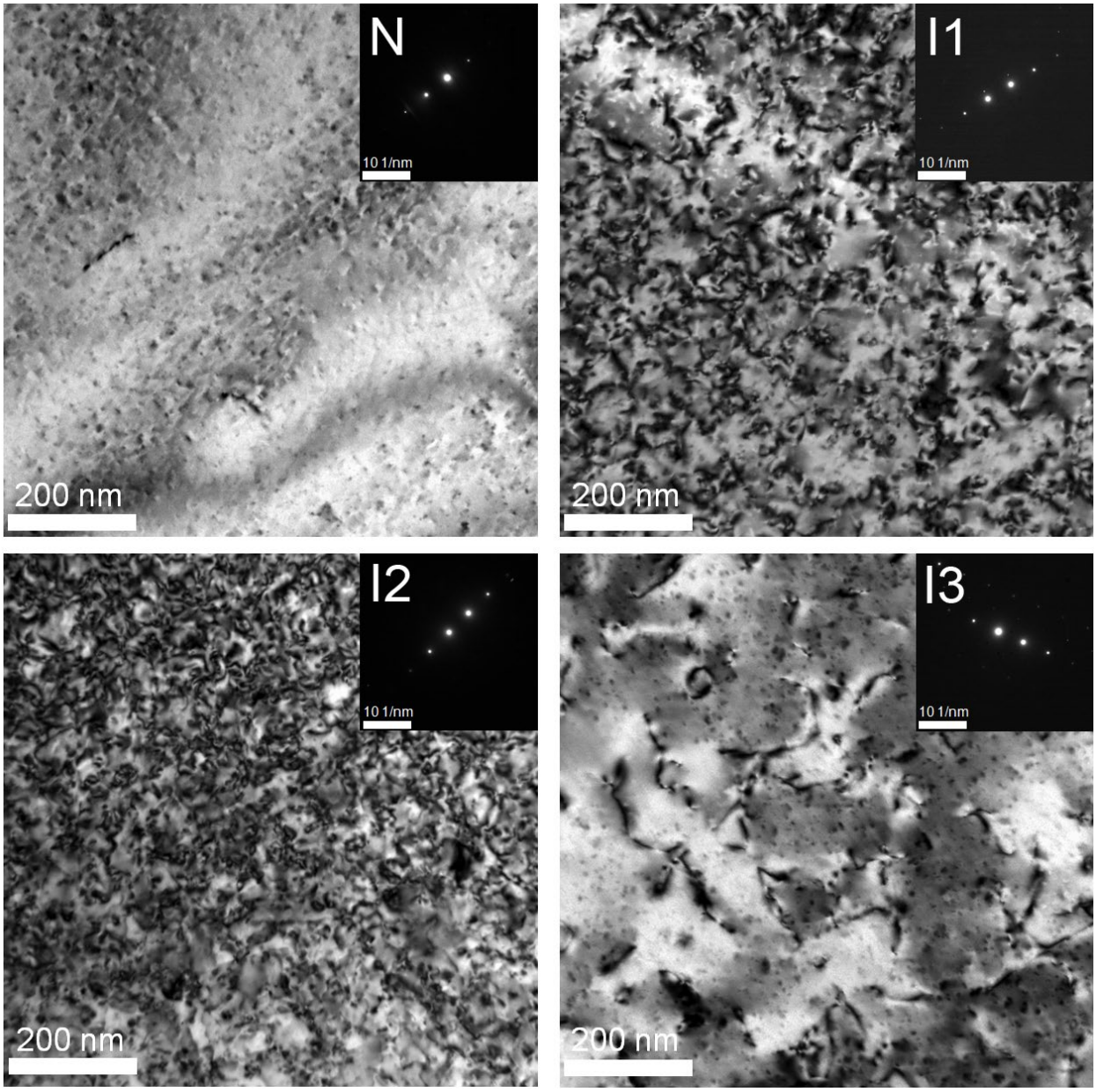

Figure 7. TEM of (N) non-irradiated MgO has minor ion damage due to the FIB and (I1) MgO has a high density of small dislocations due to neutron irradiation. TEM of (I2) MgO has a higher density of dislocations compared to (I1) MgO because of the larger irradiation dose. TEM of (I3) MgO has a lower density of larger dislocations due to the higher irradiation temperature. Each TEM image is in the **g** = [200] two-beam condition.

MgO I2 and I3 samples were thermally annealed at 1673 K for 1 h in argon, prepared by FIB, and then examined by TEM. After annealing I3 (high irradiation temperature) MgO, by visual inspection of the TEM, there were large faceted voids that were greater than 100 nm present in the bulk, which was suggested to be formed by vacancy condensation [31]. Voids less than 50 nm were present in I2 on the grain boundary. Annealing of I2 (but not I3) caused the vacancies to coalesce into voids approximately 4 nm in the bulk shown in Figure 5. It was observed that the number of dislocations decreased and the length of dislocations increased for both I2 and I3. It has been previously reported that loops disappear after annealing at 1623 K in air [32] and at 1773 K in argon [33]. Therefore, these TEM studies on the annealed samples indicate that the thermal diffusivity would recover but not to the level of the non-irradiated MgO because of the presence of voids and dislocations.

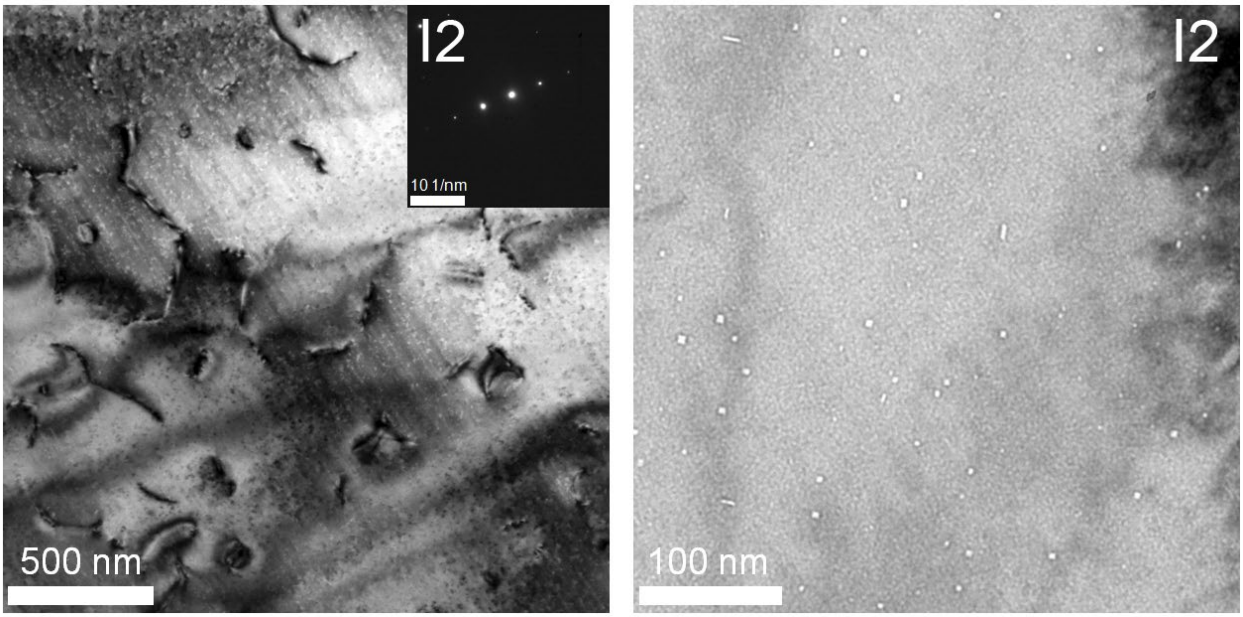

Figure 8. TEM two-beam image (**g** = [200]) of I2 MgO after being annealed at 1673 K for 1h in flowing argon showing aggregated dislocations (left). Bright field TEM image of ~4 nm voids in the bulk of I2 MgO (right).

4. Conclusions

MgO is being investigated as a possible inert matrix material because of high thermal diffusivity and radiation tolerance. MgO pellets were irradiated at 623 and 973 K to fast neutron fluencies of 1 x 10^{25} (1.5 dpa) and 2 x 10^{25} n/m^2 (3 dpa) in-pile of the Advanced Test Reactor at Idaho National Laboratory. The effects of in-pile neutron irradiation temperature and dose on MgO properties are compared between non-irradiated and irradiated MgO samples. Neutron irradiation results in significant reduction in the thermal diffusivity of MgO due to irradiation-induced defects, but not due to a change in phonon-phonon scattering. The intercept of the inverse diffusivity, which indicates the number of defects, increased with irradiation dose and decreased

with the higher irradiation temperature because point defects are more effective as scattering than aggregates. The lower irradiation temperature had a more significant reduction in thermal diffusivity due to the higher density of irradiation damage. The higher irradiation temperature increases interstitial diffusion, leading to aggregation of dislocations, which can be seen by the lack of damage around dislocation structures. The higher irradiation temperature also increases recombination, resulting in a lower dislocation density. Annealing of MgO caused vacancy-interstitial recombination, interstitial dislocation growth, and coalescence of vacancies into voids.

5. Acknowledgements

The authors would like to thank Todd Allen, James Cole, Randall Fielding, Bryan Forsmann, Collin Knight, James Madden, Thomas O'Holleran, Mary Catherine Thelen, and others at Idaho National Lab for their contributions to the project. Work supported by the U. S. Department of Energy, Office of Nuclear Energy under DOE Idaho Operations Office Contract DE-AC07-051D14517, as part of an ATR National Scientific User Facility experiment.

6. References

[1] C. Degueldre, T. Yamashita, Inert matrix fuel strategies in the nuclear fuel cycle: the status of the initiative efforts at the 8th Inert Matrix Fuel Workshop, J Nucl Mater, 319 (2003) 1-5.
[2] N. Chauvin, R.J.M. Konings, H. Matzke, Optimisation of inert matrix fuel concepts for americium transmutation, J Nucl Mater, 274 (1999) 105-111.
[3] T. Yamashita, K. Kuramoto, H. Akie, Y. Nakano, N. Nitani, T. Nakamura, K. Kusagaya, T. Ohmichi, Rock-like oxide fuels and their burning in LWRs, J Nucl Sci Technol, 39 (2002) 865-871.
[4] V.M. Oversby, C.C. McPheeters, C. Degueldre, J.M. Paratte, Control of civilian plutonium inventories using burning in a non-fertile fuel, J Nucl Mater, 245 (1997) 17-26.

[5] C. Degueldre, J.M. Paratte, Concepts for an inert matrix fuel, an overview, J Nucl Mater, 274 (1999) 1-6.
[6] C. Ronchi, J.P. Ottaviani, C. Degueldre, R. Calabrese, Thermophysical properties of inert matrix fuels for actinide transmutation, J Nucl Mater, 320 (2003) 54-65.
[7] C. Ronchi, M. Sheindlin, Melting point of MgO, J Appl Phys, 90 (2001) 3325-3331.
[8] Development of LWR fuels with enhanced accident tolerance, in, DOE Idaho Operations Office, 2012.
[9] P.G. Medvedev, S.M. Frank, T.P. O'Holleran, M.K. Meyer, Dual phase MgO-ZrO_2 ceramics for use in LWR inert matrix fuel, J Nucl Mater, 342 (2005) 48-62.
[10] P. Xu, S.J. Yates, J.C. Nino, Hydrothermal corrosion of magnesia-pyrochlore composites for inert matrix materials, J Compos Mater, 44 (2010) 1533-1545.
[11] R. Chawla, R.J.M. Konings, Categorisation and priorities for future research on inert matrix fuels: An extended synthesis of the panel discussions, Prog Nucl Energ, 38 (2001) 455-458.
[12] J.W. Gardner, A.C. Anderson, Effect of neutron irradiation on the low-temperature specific heat and thermal conductivity of magnesium oxide, Phys. Rev. B: Condens. Matter, 23 (1981) 1988-1991.
[13] R.E. Jaeger, Thermal conductivity of neutron irradiated Al_2O_3, BeO, and MgO at low temperatures, Am Ceram Soc Bull, 46 (1967) 795.
[14] D.S. Kupperman, G. Kurz, H. Weinstock, Thermal-conductivity of neutron-irradiated MgO, J Low Temp Phys, 10 (1973) 193-201.
[15] P. Xu, P.E. Murray, Thermal analysis of ATR-NSUF University of Florida experiment, in, 2008.
[16] Advanced Test Reactor National Scientific User Facility users' guide, in, Idaho National Laboratory, 2009.
[17] P. Medvedev, J.C. Nino, J.A. Foster, Irradiation test plan for the ATR National Scientific User Facility - University of Florida project, in, 2008.
[18] S.J. Zinkle, C. Kinoshita, Defect production in ceramics, J Nucl Mater, 251 (1997) 200-217.
[19] L.M. Clark, R.E. Taylor, Radiation loss in flash method for thermal-diffusivity, J Appl Phys, 46 (1975) 714-719.
[20] B. Henderson, D.H. Bowen, Radiation damage in magnesium oxide. 1. Dose dependence of reactor damage, J Phys Part C Solid, 4 (1971) 1487.
[21] T. Ungár, Microstructural parameters from X-ray diffraction peak broadening, Scripta Materialia, 51 (2004) 777-781.
[22] C.J. Howard, T.M. Sabine, X-Ray diffraction profiles from neutron irradiated magnesium oxide, J Phys C Solid State, 7 (1974) 3453-3466.
[23] F.W. Clinard, Ceramics for applications in fusion systems, J Nucl Mater, 85-6 (1979) 393-404.
[24] F.W. Clinard, G.F. Hurley, L.W. Hobbs, Neutron-irradiation damage in MgO, Al_2O_3, and $MgAl_2O_4$ ceramics, J Nucl Mater, 108 (1982) 655-670.
[25] D.J. Senor, G.E. Youngblood, L.R. Greenwood, D.V. Archer, D.L. Alexander, M.C. Chen, G.A. Newsome, Defect structure and evolution in silicon carbide irradiated to 1 dpa-SiC at 1100 degrees C, J Nucl Mater, 317 (2003) 145-159.

[26] R.J. Bruls, H.T. Hintzen, R. Metselaar, A new estimation method for the intrinsic thermal conductivity of nonmetallic compounds - A case study for $MgSiN_2$, AlN, and beta-Si_3N_4 ceramics, J Eur Ceram Soc, 25 (2005) 767-779.
[27] M. Akiyoshi, Thermal diffusivity of ceramics at the neutron irradiation temperature estimated from post-irradiation measurements at 123-413 K, J Nucl Mater, 386-88 (2009) 303-306.
[28] P.G. Klemens, Theory of Thermal Conduction in Dielectric Solids - Effects of Radiation-Damage, Nucl Instrum Meth B, 1 (1984) 204-208.
[29] R.J. Price, Thermal-conductivity of neutron-irradiated pyrolytic beta-silicon carbide, J Nucl Mater, 46 (1973) 268-272.
[30] R.S. Wilks, Neutron-induced damage in BeO, Al_2O_3, and MgO - a review, J Nucl Mater, 26 (1968) 137-173.
[31] C.S. Morgan, D.H. Bowen, Inert gas bubbles in neutron-irradiated magnesium oxide, Philos Mag, 16 (1967) 165.
[32] G.W. Groves, A. Kelly, Prismatic dislocation loops in cold-worked and annealed MgO crystals, J Appl Phys, 34 (1963) 3104-3107.
[33] D.H. Bowen, F.J.P. Clarke, Growth of neutron irradiated magnesium oxide, Philos Mag, 9 (1964) 413.